2004

# A perfectly matched layer approach to the linearized shallow water equations models

Navon, I.M.

# A perfectly matched layer approach to the linearized shallow water equations models

I.M. Navon*
Department of Mathematics and
Computational Science and Information Technology
Florida State University
Tallahassee, FL 32306-4130
Email: navon@csit.fsu.edu

B. Neta
Naval Postgraduate School
Department of Mathematics
Monterey, CA 93943

M.Y. Hussaini
Computational Science and Information Technology
Florida State University
Tallahassee, FL 32306-4120

December 3, 2003

*Corresponding author

**Abstract**

A limited-area model of linearized shallow water equations (SWE) on an $f$-plane for a rectangular domain is considered. The rectangular domain is extended to include the so-called perfectly matched layer (PML) as an absorbing boundary condition. Following the proponent of the original method, the equations are obtained in this layer by splitting the shallow water equations in the coordinate directions and introducing the absorption coefficients. The performance of the PML as an absorbing boundary treatment is demonstrated using a commonly employed bell-shaped Gaussian initially introduced at the center of the rectangular physical domain.

Three typical cases are studied:

- A stationary Gaussian where adjustment waves radiate out of the area.
- A geostrophically balanced disturbance being advected through the boundary parallel to the PML. This advective case has an analytical solution allowing us to compare forecasts.
- The same bell being advected at an angle of 45 degrees so that it leaves the domain through a corner.

For the purpose of comparison, a reference solution is obtained on a fine grid on the extended domain with the characteristic boundary conditions. We also compute the r.m.s. difference between the 48-hour forecast and the analytical solution as well as the 48-hour evolution of the mean absolute divergence which is related to geostrophic balance. We found that the PML equations for the linearized shallow water equations on an $f$-plane support unstable solutions when the mean flow is not unidirectional. Use of a damping term consisting of a 9-point smoother added to the discretized PML equations stabilizes the PML equations. The reflection/transmission is analyzed along with the case of instability for glancing propagation of the bell disturbance. A

numerical illustration is provided showing that the stabilized PML for glancing bell propagation performs well with the addition of the damping term.

# 1 Introduction

In a limited-area numerical weather prediction model, the lateral boundaries are not physical boundaries, and they require artificial boundary conditions so that the problem is well-posed and the solution in the limited area remains uncontaminated and consistent with the global solution. As such the treatment of lateral boundaries with the non-reflecting or absorbing boundary conditions has been the subject of continuing interest since the early days of numerical weather prediction.

Several good reviews are available on the topic of both physical and artificial boundary conditions (Givoli and Harari, 1998; Turkel, 1983; Givoli, 1991; Mcdonald, 1997; and Tsynkov, 1998). Givoli and Harari (1998) have edited a special issue of Computer Methods in Applied Mechanics and Engineering on the subject of boundary conditions for exterior wave propagation problems. Turkel (1983) provided an early review on the outflow boundary conditions in the context of computational aerodynamics. Givoli (1991) reviews nonreflecting boundary conditions for the wave problems, discusses local and nonlocal boundary conditions for physical and artificial boundaries in the context of problems from different disciplines. McDonald's (1997) review is confined to lateral boundary conditions for operational regional forecast models. Kalnay (2001) presents the state of art of limited area boundary conditions as used in meteorology. The most comprehensive survey to date of artificial boundary conditions is due to Tsynkov (1998). He provides a comparative assessment of the current methods for constructing the artificial boundary conditions and divides them into two categories – local and global artificial boundary conditions. Global artificial boundary conditions are so called because they involve integral transforms along the artificial boundary. For example, the approaches of Givoli and Keller (1989) typify the global artificial boundary conditions. Such boundary conditions seem to work only in specific geometries. In addition, discretization by a finite element method results in the filling of dense blocks in an otherwise sparse system. On the other hand, local artificial boundary conditions preserve the sparsity of

the problem, e.g. Sommerfeld radiation condition and the traditional characteristic boundary conditions. Typical examples of local approaches to artificial boundary conditions are those of Gustafsson and Sundström (1978) and Engquist and Majda (1977, 1979). The so-called transparent boundary conditions of McDonald (2001a, 2001b, 2002) and of Holstad and Lie (2001) and Lie (2001) applied to the shallow water equations also belong to this category.

The buffer/sponge layer consists in surrounding the truncated physical domain with a zone in which non-physical equations are employed to filter or damp incident waves so that there is minimal reflection into the physical domain of interest (see Kar and Turco, 1995). The boundary relaxation scheme of Davies (1976, 1983) is such an approach, and it is most frequently used for limited area forecasting using mesoscale model.

The perfectly matched layer (PML) method recently introduced by Berenger (1994) as an absorbing boundary condition in the context of electromagnetic wave propagation has the property of absorbing incident waves irrespective of their frequency and orientation. The parameters of the PML are chosen such that the wave either never reaches the external boundary, or, even if it reaches the boundary and reflects back, its amplitude is negligibly small by the time it reaches the interface between the absorbing layer and interior domain. Hu (1996a) was the first to apply the PML approach to aeroacoustic problems using the linearized Euler equations then (1996b) extending his work to nonuniform mean flow for the nonlinear Euler equations. (Clement, 1996; Karni, 1996; R. Kosloff and D. Kosloff,1986; Collino, 1997; Hayder *et al.*, 1999; Hayder and Atkins, 1997). The work of Hayder *et al.* (1999) is the first to demonstrate the viability of the PML method in the applications! to nonlinear Euler equations. A preliminary work of Darblade *et al.* (1997) implements the PML method to the linearized shallow water equations model in oceanography.

Hu (2001) presents a new stable PML formulation for the linearized Euler equations in unsplit physical variables and provides a modification to render the proposed scheme strongly well-posed by the addition of arbitrarily small terms. Abarbanel and Gottlieb (1997) provide

the general mathematical analysis of the PML method while Abarbanel *et al* (1999) provide a well posed version of PML for advective acoustics. Abarbanel and Gottlieb (1998) provide the mathematical framework for use of PML in computational acoustics. The well posedness of PML for linearized Euler equation and for the Cauchy problem is discussed in Rahmouni (2000) and Metral and Vacus (1999), respectively. The PML approach has been shown to provide significantly better accuracy than most other artificial boundary conditions in many applications.

The paper is organized as follows. In section 2, we introduce the PML approach to the linearized two-dimensional shallow-water equations on an $f$-plane for the purpose of analysis. Using a MAPLE symbolic manipulator we obtain a dispersion relation for the linearized PML split shallow water equations system.

In Chapter 3 we provide a description of the numerical testing using a widely employed bell shape Gaussian (McDonald, 2000) at the center of the domain. The first test consists of an adjustment case which is not in geostrophic balance and we compare the PML results with its known asymptotic solution.

We then proceed to test an advective case of the bell shape Gaussian propagating in parallel to the PML. This case has an analytical solution with which we can compare our forecasts in terms of rms error as well as the vanishing of the mean absolute divergence. Note that since the system is in geostrophic balance, the analytical divergence on a constant $f$ plane is always zero.

This is followed by a test of propagation of the bell shaped Gaussian at an angle with the PML yielding unstable solutions of the PML equations, (see also Hu, 1996a; Tam *et al.*, 1998). An analysis is carried out to understand and explain the underlying reasons for the instability. Application of a 9-point Laplacian filter stabilizes the PML.

# 2 The perfectly matched layer methodology

In this section we will briefly present the framework of the PML method for the linearized shallow-water (S-W) equations on an $f$-plane.

## 2.1 Linearized S-W equations on an $f$ plane

The 2-D linearized shallow water model on an $f$-plane is of the form

$$\frac{\partial}{\partial t}u + U\frac{\partial}{\partial x}u + V\frac{\partial}{\partial y}u + \frac{\partial}{\partial x}\phi - fv = 0 \tag{1}$$

$$\frac{\partial}{\partial t}v + U\frac{\partial}{\partial x}v + V\frac{\partial}{\partial y}v + \frac{\partial}{\partial y}\phi + fu = 0 \tag{2}$$

$$\frac{\partial}{\partial t}\phi + U\frac{\partial}{\partial x}\phi + V\frac{\partial}{\partial y}\phi + \Phi(\frac{\partial u}{\partial x} + \frac{\partial v}{\partial y}) = 0 \tag{3}$$

where $U = U_{mean}$ and $V = V_{mean}$ are constants and $\Phi$ is the mean geopotential height. If we put $V = 0$, $f = 0$, and scale the geopotential, we get the linearized Euler equations used by Hu (1996b). Thus the results of Hu (1996b) are applicable to this form of the linearized S-W equations (not including Coriolis).

## 2.2 The split-PML linearized shallow water equations on the $f$ plane

The inclusion of the Coriolis factor in the linearized shallow-water equations about $(U, V)$ requires the following modification of the PML split form given by Hu (1996b):

$$
\begin{aligned}
&\frac{\partial u_1}{\partial t} + U\frac{\partial u}{\partial x} + \frac{\partial \phi}{\partial x} = -\sigma_x u_1 \\
&\frac{\partial u_2}{\partial t} + V\frac{\partial u}{\partial y} = -\sigma_y u_2 \\
&\frac{\partial u_3}{\partial t} - fv = 0 \\
&\frac{\partial v_1}{\partial t} + U\frac{\partial v}{\partial x} = -\sigma_x v_1 \\
&\frac{\partial v_2}{\partial t} + V\frac{\partial v}{\partial y} + \frac{\partial \phi}{\partial y} = -\sigma_y v_2 \\
&\frac{\partial v_3}{\partial t} + fu = 0 \\
&\frac{\partial \phi_1}{\partial t} + \Phi\frac{\partial u}{\partial x} + U\frac{\partial \phi}{\partial x} = -\sigma_x \phi_1 \\
&\frac{\partial \phi_2}{\partial t} + \Phi\frac{\partial v}{\partial y} + V\frac{\partial \phi}{\partial y} = -\sigma_y \phi_2
\end{aligned}
\tag{4}
$$

In the above the coefficients $\sigma_x$ and $\sigma_y$ have been introduced for the absorption of waves in the PML. We will refer to them as absorption coefficients in this work and they will be assumed to be non negative. In general, these coefficients are not constant, see later, but in the analysis in this section will assume constant absorption coefficients. We notice that when

$$\sigma_x = \sigma_y = 0 \tag{5}$$

we are reduced to the original linearized 2-D shallow-water equations with

$$u = u_1 + u_2 + u_3 \tag{6}$$

$$v = v_1 + v_2 + v_3 \tag{7}$$

$$\phi = \phi_1 + \phi_2 \tag{8}$$

The spatial derivatives involve only the total fields of $u$, $v$ and $\phi$ which are assumed to be continuous at the interface between the interior domain and the PML. Two types of interfaces

are being created, namely, the interfaces between the interior domain and the PML domain and those between two adjacent PML domains, see the following diagram.

| $PML$ $(0,\sigma_y)$ | $(\sigma_x,\sigma_y)$ |
|---|---|
| $(0,0)$ | $(\sigma_x,0)$ |
| interior | $PML$ |

A similar approach was used for the linearized shallow-water equations in oceanography by Darblade *et al.* (1997). If we use the split suggested by Hu (1996a), the linearized system will have a solution $u_2 = 0$ and thus as if we didn't split the $u$ variable in the PML.

The dispersion relation (see Darblade, 1997) between possibly complex wavevector $(k_x, k_y)$ and possibly complex frequency $\omega$ can be obtained (using MAPLE symbolic manipulator)

$$-\omega^2 W_x^3 W_y^3 Z \left[\Phi(X^2+Y^2) - F^2 + Z^2\right] = 0 \tag{9}$$

where

$$Z = 1 + iUX \tag{10}$$

$$W_x = \sigma_x - i\omega,\ W_y = \sigma_y - i\omega \tag{11}$$

$$X = \frac{k_x}{W_x},\ Y = \frac{k_y}{W_y},\ F = \frac{f}{\omega}. \tag{12}$$

These equations imply that $W_x$ and $W_y$ are not zero, but the vanishing of these variables is included in (9). In the case we include the terms with $V$, the dispersion relation will be the same except for $Z$ which will depend on $V$ as follows

$$Z = 1 + iUX + iVY. \tag{13}$$

The solution of the dispersion equation (9) can have stable and unstable solutions.

## 2.3 Reflection and transmission at an interface between two domains

We quote here the necessary conditions for perfect transmission of plane waves at the interface between 2 distinct domains, $D_1$, and $D_2$. This includes the interface between the interior limited area domain and the PML domain, see Darblade (1997).

The linearized S-W equations can be viewed as the split field PML linearized S-W equations with both absorption coefficients being zero across an interface normal to $x$ and $y$ between an interior domain and a PML domain.

Following Darblade (1997), we let the interface $\Gamma$ between the two domains $D_1$ and $D_2$ be a line $x = x_0$. Let $\sigma_{x_i}$, $\sigma_{y_i}$, $i = 1, 2$ be the absorption coefficients in the $x, y$ directions in $D_i$. The variables $u, v, \phi$ are continuous across the interface $\Gamma$. The necessary conditions for the perfect transmission at the interface of plane wave in the form

$$\psi = \Psi_0 \, e^{i(k_x x + k_y y - \omega t)}$$

where $\psi = (u_1, u_2, u_3, v_1, v_2, v_3, \phi_1, \phi_2)$ is the solution of (4) if

1. The triplet $(\omega, k_x, k_y)$ satisfies the dispersion equation (9)

2. The amplitudes $\Psi_0$ are the solution of the linear homogeneous system for which the determinant is the dispersion equation (9).

The sufficient condition for perfect transmission is $\sigma_{y_1} = \sigma_{y_2}$. Note that if the interface is parallel to the $y$ axis, the condition becomes $\sigma_{x_1} = \sigma_{x_2}$.

# 3 Numerical testing

A 2-D linearized shallow-water equations solver based on the explicit time differencing scheme of Miller-Pearce is used (see Appendix of Miller and Pearce, 1974). This scheme is implemented on a non-staggered grid but provides a fair comparison since all methods are tested using the same discretization. The scheme has a CFL stability condition

$$\Delta t \leq \frac{\sqrt{(\Delta x)^2 + (\Delta y)^2}}{\sqrt{\Phi}\sqrt{2}}$$

Spatial differencing of the linearized shallow water equations was carried out on a rectangular domain of $141 \times 141$ grid points, with a uniform spatial horizontal grid length of $\Delta x = \Delta y =$

$100km$. We used values of $H = h_{av} = 5000m$ and a time step of $\Delta t = 120sec$. At the outer boundary of the PML domain we apply characteristic boundary conditions. On the boundary line we imposed $\phi - \sqrt{\Phi}\, v_N$ at all points and $v_T$ at the inflow points, where $v_N$ and $v_T$ are the outward normal and tangential components of velocity, respectively.

We compared the results with a control simulation computed on a much larger domain of 400 by 400 grid points which is not affected by the boundary conditions for the integration time span. The PML domain contains points $(x,\, y)$ such that $50 < |x|/\Delta x < 70$ and $50 < |y|/\Delta y < 70$.

## 3.1 Testing Adjustment case

We investigated the permeability of the boundaries for the PML case for the linearized shallow-water equations. The initial state considered is with $\nabla\phi(x, y, 0) \neq 0$ and $u(x, y, 0) = v(x, y, 0) = 0$. Since the system is not in geostrophic balance, the system radiates adjustment gravity waves and it will adjust to a balanced state given by the stream function $\psi(x, y)$ which satisfies the equation

$$\left(\frac{\partial^2}{\partial x^2} + \frac{\partial^2}{\partial y^2} - \frac{f^2}{\Phi}\right)\psi(x, y) \;=\; -\frac{f^2}{\Phi}\phi(x, y, 0) \tag{14}$$

See Gill (1982, section 7.2.2) for details and McDonald (2002). For all our numerical tests we used $\Delta x = \Delta y = 100km$ and $L_x = L_y = 10,000km$. In all the tests conducted, we used $\Phi = (5000m)\, g$, and $\hat{\phi} = (500m)\, g$. The experiment starts with a bell-shaped Gaussian at the center of the domain

$$\phi(x, y, 0) = \Phi + \hat{\phi} \exp\left\{-\left[\frac{x - L_x/2}{L_x/10}\right]^2\right\} \exp\left\{-\left[\frac{y - L_y/2}{L_y/10}\right]^2\right\} \tag{15}$$

with $u(x, y, 0) = v(x, y, 0) = 0$ and the advecting velocities $U, V$ are also set to zero. The adjustment process radiates away gravity waves from the center of the domain.

The absorption coefficients are varied gradually inside the PML. Typically, one uses

$$\sigma_x = \sigma_m \left|\frac{x - x_\ell}{D}\right|^\gamma,\;\; \sigma_y = \sigma_m \left|\frac{y - y_\ell}{D}\right|^\gamma, \tag{16}$$

where $x_\ell$, $y_\ell$ denote the location where the PML starts, $D$ is the depth of the layer, $\gamma$ is a constant (see Hu, 1996b). A PML of depth of only $20\Delta x$, was used where the parameters governing the spatial variation of $\sigma_x$, $\sigma_y$ for the absorbing layer were $\gamma = 3$ and $\sigma_m = 0.0018$. The asymptotic state arrived at by solving the balance equation (14) is compared as in McDonald (2002) with the 48-hour forecasts to assess the transparency of the boundaries.

We display in Fig. 1 various stages of the adjustment process showing that $h(x, y, t)$ is always circularly symmetric. At the top left plot we show the initial condition, a Gaussian bell at the center of the domain. At the top right plot one can see the solution after 6 hours. The bottom plot gives the solution after 42 hours. The rms differences between a 48-hour forecast and the asymptotic solution given by the balanced state are provided in Table 1. This balanced state arrived at by solving (14) with $\phi(x, y, 0)$ given by (15) and $\psi = (5000m)g$ on the boundary is not displayed, but visually identical to the 48 hour forecast shown in the bottom plot of Figure 1.

These results show that the boundaries are almost transparent to the adjustment waves, that is, the waves exit without reflection. The forecast is almost identical to the the asymptotic balanced state described in McDonald (2002).

A graph of the mean absolute divergence (in $\sec^{-1}$) multiplied by $10^8$ is displayed for the propagation of the bell-shaped Gaussian for the case of adjustment is provided in Fig. 2. The absolute value of divergence is displayed for the small domain with PML case, small domain without PML and large domain. The results of PML case and the large domain are practically indistinguishable for up to $t = 48$ hours. The case of no PML shows large deviations starting at $t = 14$ hours but later settles to the common value at about $t = 42$ hours.

## 3.2 Testing Advection with PML

The linearized shallow water equations are given by (1)-(3) and have an analytic solution describing advection of a bell-shaped Gaussian with constant velocity $(U, V)$ starting from center of domain at position $(x_c, y_c)$. Thus we have an analytical solution to compare propagation of the Gaussian using the PML approach. The analytical solution for the bell-shaped Gaussian takes the form

$$\phi(x, y, t) = \Phi + \hat{\phi} \exp\left\{ -\left[ \frac{x - x_c - Ut}{L_x/10} \right]^2 \right\} \exp\left\{ -\left[ \frac{y - y_c - Vt}{L_y/10} \right]^2 \right\} \tag{17}$$

with $(u, v)$ in geostrophic balance. As mentioned by McDonald (2002) the analytic divergence is zero, and so this provides an additional test of the efficacy of the scheme used.

We tested the split PML for 2 cases, one is a wave propagating parallel to the $x$-axis and the other at an angle of 45° with it.

1. **Propagation parallel to the PML $x$ axis**

   PML of 20 grid points, $U = 50m/sec$, $\sigma_m = .0018$, $\gamma = 3$, $f$ plane and $\theta = 30°$ where $\theta$ is the latitude at which the Coriolis factor is calculated. A plot of the evolution of the advection of the bell-shaped Gaussian out of the area using the PML is provided. We display it for a period of integration of 39 hours in Fig. 3. The figure shows that $h(x, y, t)$ is approximately a decaying translating Gaussian. We see that the PML layer is very effective and performs well as an absorbing boundary condition. The root-mean squared difference between the 48 hour forecast and the analytical solution is provided in Table 2.

   A graph of the mean absolute divergence (in $\sec^{-1}$) multiplied by $10^8$ for the propagation of the bell-shaped Gaussian for the case of propagation parallel to the PML is presented in Fig. 4. The results of all 3 cases coincide for the first 32 hours. The results of the PML coincide with those of the large domain for the 48 hour forecast

whereas the results in the small region without PML show a big increase as the bell reaches the boundary (Fig. 4). As the bell reaches the boundary, the mean absolute divergence for the case without PML drastically increase, while the other two cases tend to nondivergence as in the analytical solution.

2. **Propagation of bell-shaped Gaussian at an angle of** $45^\circ$

   We start with the bell-shaped Gaussian at the center of the domain and advect it so that it exits through a corner, i.e. $(x_c, y_c) = (L_x/2, L_y/2)$ and $(U, V) = (50m/sec, 50m/sec)$ thus ensuring that the Gaussian exits at the corner defined by $(L_x, L_y)$.

   In the implementation of the PML as an absorbing boundary condition we used a $\sigma$ curve very similar to that used by Tam et al. (1998). The $\sigma$ curve (see Fig. 8) starts with a value of $\sigma = 0$ at the fifth mesh point from the interface between the computational domain and the PML. It is then followed by 8 mesh points where a cubic spline curve is used until the full value of $\sigma_x = \sigma_y = \sigma_m$ is attained . This was important for the case where artificial damping was used in the case where the bell was propagating at an angle.

   We present graphically the generation of instabilities in the PML for this case. As a cure to instabilities manifested (confined) primarily to short waves, we applied a 9-point smoother in the PML

$$u_{ij} \leftarrow \sum_{k=-1}^{1} \sum_{\ell=-1}^{1} \frac{u_{i+k\ j+\ell}}{2^{2+|k|+|\ell|}} \tag{18}$$

Figure 5 shows the propagation of the Gaussian bell at an angle of $45^\circ$. We have shown the solution at 24 and 36 hours. The intial solution is the same as in top left of Figure 3. Since the advection speed is $50m/sec$ in each direction, the Gaussian bell is travelling along the diagonal from the center of the domain. Compare top left plot of Figure 5 to top right plot of Figure 3. Figure 7 shows the 2-D plot of the Gaussian bell propagating at an angle with and without a 9-point smoother after 60 hours of forecast. Without the smoother the

growth of the excited unstable solution spreads back into the interior computational domain (bottom plot of Fig. 7) whereas using artificial damping provided by the 9 point Laplacian is effective in suppressing the instabilities of the PML equations. This filter continuously damps the instabilities once they propagate into the PML (top right plot of Fig. 7).

A graph of the mean absolute divergence (in $\sec^{-1}$) multiplied by $10^8$ for the propagation of the bell-shaped Gaussian for the case of propagation at an angle of 45° to the PML is presented in Fig. 6. The results agree up to $t = 34$ hours and then display small variations probably due to use of 9-point smoother.

# 4 Summary and conclusions

In this paper we have described and implemented the PML split equations approach for the linearized shallow water equations based on an explicit Miller-Pearce scheme finite difference discretization (see Appendix of Miller and Pearce, 1974).

The split PML approach was tested for its efficiency as an absorbing boundary condition for the linearized shallow water equations using three different scenarios. First we tested permeability of the PML absorbing boundary conditions to adjustment waves. Measured against an asymptotic balanced state we found small rms errors for the 48-hour forecast in the same range as those found by Mc Donald (2002). The rms between the 48h forecast and the asymptotic solution are only slightly larger than those obtained in the best case of McDonald (2002). This may be attributed to our use of a grid-A model.

In a second scenario we tested the split-PML for advection of the bell shape - viewed as a geostrophically balanced sharp pseudo-meteorological feature (McDonald, 2002) for 2 separate cases, both starting with a bell-shaped Gaussian at the center of the computational domain.

a) the mean flow is parallel to the PML layer.

b) propagation at an angle of 45° exiting through a corner.

An analysis similar to that of Tam *et al.* (1998) finds that in such case (i.e. propagation at an angle, when the mean flow is not unidirectional) the split PML for linearized shallow water equations supports unstable solutions. Application of a 9-point Laplacian filter stabilizes the PML. Our numerical experiments show that the stabilized PML performs well as an absorbing boundary condition for the linearized shallow water equations including the Coriolis factor. Our results compare well with those obtained by Mc Donald (2002) for the same case.

The research carried out here has a natural extension to the formulation of boundary conditions for advanced mesoscale models, such as the MM5 and the new MRF models, and may improve upon the combination of nudging and sponge layer presently used in such models. Work with PML in the framework of mesoscale models will mean that gravity waves can not only leave the domain but also enter it without hindrance (McDonald, 2003).

Our results are encouraging and constitute a step towards using the PML absorbing boundary conditions for full 3D atmospheric and ocean models. One avenue to achieve this goal is to implement the PML boundary conditions to a 3D multi-layer shallow water equations model as a way to proceed towards full 3D models. This can be done for the linearized hydrostatic equations by carrying out a normal mode decomposition yielding a shallow water equation for each vertical mode.

Development of a non-split version of both the linearized and the nonlinear version of the shallow water equations based on ideas put forward by Abarbanel and Gottlieb (1998), Abarbanel *et al.* (1999) and Hesthaven (1998) is presently also being investigated.

**Acknowledgments**

The first author would like to express his gratitude for the support extended to him by the Center of Excellence (COE) at Florida State University during part of the write-up of this paper. This is a contribution from the climate institute, a center of excellence funded by the FSU research foundation.He also acknowledges support from NSF grant ATM-97B1472

managed by Dr. Pamela Stephens. He would also like to express his gratitude for the support and encouragement provided to him during his short stay at NCAR, fall 1999 made possible by DR Ying-Hwa Kuo, Head Mesoscale Prediction Group and by Dr Joseph Klemp, Head Mesoscale Dynamics Group both at NCAR/MMM. The expert programming help provided by Dr Zhuo Liu during the implementation stages at C.S.I.T. is gratefully acknowledged. The useful discussion with Dr Sajal K. Kar is acknowledged. The secretarial support and the expert librarian support at NCAR is also acknowledged. The authors greatly appreciate the referees work i! mproving the paper.

# REFERENCES


Abarbanel, S. and D. Gottlieb, 1997: A mathematical analysis of the PML method, *J. Comput. Phys.*, **134**, 357-363.

Abarbanel, S. and D. Gottlieb, 1998: On the construction and analysis of absorbing layers in CEM, *Appl. Numer. Math.*, **27**, 331-340.

Abarbanel, S., Gottlieb, D. and J. S. Hesthaven, 1999: Well-posed perfectly matched layers for advective acoustics, *J. Comput. Phys.*, **154**, 266-283.

Berenger,J. -P., 1994:A perfectly matched layer for the absorption of electromagnetic waves, *J. Comput. Phys.*, **114**, 185-200.

Clement, A., 1996: Coupling of two absorbing boundary condition for 2D time-domain simulation of free surface gravity waves, *J. Comput. Phys.*, **126**, 139-151.

Collino, F., 1997: Perfectly matched absorbing layers for paralaxial equations, *J. Comput. Phys.*, **131**, 164-180.

Darblade, G. ,1997: Methodés Numeriqués et Conditions aux Limites pour les Modèles Shallow Water Multicouches, Ph. D. Thesis, Université de Bordeaux I, Groupe de Recherche en Analyse et Modèlisation Mathématique. ( Available from Prof A. Y. LeRoux, Institut de Mathématiques, Université Bordeaux I, F-33405 Talence, FRANCE)

Darblade, G., Baraille, R., le Roux, A.-Y., Carton, X. and D. Pinchon, 1997: Conditions limites non réfléchissantes pour un modèle de Saint-Venant bidimensionnel barotrope linéarisé, *C. R. Acad. Sci. Paris*, **324**, 485-490.

Davies, H. C., 1976: A lateral boundary formulation for multilevel prediction models, *Quart. J. Roy. Meteor. Soc.*, **102**, 405-418.

Davies, H. C., 1983: Limitations of some common lateral boundary schemes used in regional NWP models, *Mon. Wea. Rev.*, **111**, 1002-1012.

Engquist, B. and A. Majda, 1977: Absorbing boundary conditions for the numerical simulation of waves, *Math. Comp.*, **31**, no 139, 629-651.

Engquist, B. and A. Majda, 1979: Radiation boundary conditions for acoustic and elastic wave calculations, *Comm. Pure. Appl. Math.*, **32**, 313-357.

Gill, A. E., 1982: Atmosphere-Ocean Dynamics. Academic Press, New York.

Givoli, D., 1991: Nonreflecting boundary conditions, *J. Comput. Phys.*, **94**, 1-29.

Givoli, D., and J. B. Keller,1989: A Finite element method for large domains,*Comput. Meths. Appl. Mech. Eng.*, **76**, 41-66.

Givoli, D. and I. Harari, guest editors, 1998: Exterior problems of wave propagation, Special issue of *Computer Methods in Applied Mechanics and Engineering*, **164(1-2)**, 272 p.

Gustafsson, B., and A. Sundström, 1978: Incompletely parabolic problems in fluid dynamics, *SIAM J. Appl. Math.*, **35**, 343-357.

Hayder, M. E. and H. L. Atkins, 1997: Experience with PML boundary conditions in fluid flow computation in T.L. Gears Ed.. Collection of Abstract of Symposium on computational methods for unbounded domains. Univ. of Colorado at Boulder, July 27-31 (Kluwer Academic Press) to appear.

Hayder, H. E., Hu, F. Q. and M. Y. Hussaini, 1999: Towards perfectly absorbing boundary conditions for Euler equations, *AIAA Journal*, **37**, no 8 , 912-918.

Hesthaven, J. S., 1998: On the analysis and construction of perfectly matched layers for the linearized Euler equations, *J. Comput. Phys.*, **142**, 129-147.

Holstad, A. and Lie, I., 2001: Transparent boundary conditions using a mixed finite element formulation of the shallow water equations, Norwegian Met. Inst. (DNMI), Research Report No. 120, 48 pp.

Hu, F. Q., 1996a: On absorbing boundary conditions for linearized Euler equations by a perfectly matched layer, *J. Comput. Phys.*, **129**, 201-219.

Hu, F. Q., 1996b: On perfectly matched layer as an absorbing boundary condition, AIAA paper 96-1664.

Hu, F. Q., 2001:A stable, perfectly matched layer for linearized Euler equations in unsplit physical variables.*J. Comput. Phys.*, **173**, 455-480.

Kalnay, E., 2001: Numerical Weather Forecasting and Predictability, Cambridge University Press, Cambridge, MA.

Kar, S.K. and R. P. Turco, 1995: Formulation of a lateral sponge layer for the limited-area shallow water models and an extension for the vertically stratified case. *Mon. Wea. Rev*, **123**, 1542-1559.

Karni, S., 1996: Far field filtering operators for suppression of reflections from artificial boundaries, *SIAM J. Numerical Analysis*, **33**, 1014-1047.

Kosloff, R. and D. Kosloff, 1986: Absorbing boundaries for wave propagation problems, *J. Comput. Phys.*, **63**, 363-376.

Lie, I., 2001: Well-posed transparent boundary conditions for the shallow water equations, *Appl. Numer. Math.*. **38**, 445-474.

McDonald, A., 1997: Lateral boundary conditions for operational regional forecast models: A review HIRLAM Technical Report No 32, 31pp.

McDonald, A., 2000:Boundary conditions for semi-Lagrangian schemes: Testing some alternatives in one-dimensional models.*Mon. Wea. Rev.*,**128 (12)**, 4084-4096.

McDonald, A., 2001a: A step toward transparent boundary conditions for meteorological models, Technical Note No. 57, 22 pp.

McDonald, A., 2001b: Well posed boundary conditions for semi-Lagrangian schemes: The two dimensional case, HIRLAM Technical Report No. 47, 38 pp.

McDonald, A., 2002: A step toward transparent boundary conditions for meteorological models, *Mon. Wea. Rev.*, **130, No. 1**, pp. 140–151.

McDonald, A., 2003: Transparent boundary conditions for the shallow water equations: testing in a nested environment, *Mon. Wea. Rev.*, **131**, 698–705.

Metral, J. and O. Vacus, 1999: Well-posedness of the Cauchy problem associated with Berenger's system, *Comp. Rendus de L'Acad. des Sci. Serie I-Math.*, **328**, 847-852.

Miller, M. J. and R. P. Pearce, 1974: A three dimensional primitive equation model of cumulonimbus convection, *Quart, J. Roy. Met. Soc*, **100**, 133-154.

Rahmouni, A., 2000: A well-posed unsplit PML model for linearized Euler equations, *Comp. Rendus de L'Acad. des Sci. Serie I-Math.*, **331**, 159-164.

Tam, C. K. W., Aurialt, L. and F. Cambuli, 1998: Perfectly matched layer as an absorbing boundary condition for the linearized Euler equations in open and ducted domains, *J. Comput. Phys.*, **144**, 213-234.

Tsynkov, S. V., 1998: Numerical solution of problems on unbounded domains. A review, *Applied Num. Math.*, **27**, 465-532.

Turkel, E., 1983: Progress in Computational Physics, *Computers and Fluids*, **11**, 121-144.

# Captions

**Fig. 1** The adjustment of a bell shape using PML absorbing boundary condition: on the top left at 0 hour, on the top right at 24 hour forecast and on the bottom at 42 hour forecast.

**Fig. 2** Graph of the mean absolute divergence (in $\sec^{-1}$) for the adjustment case multiplied by $10^8$. Case of no PML, large computational domain and a PML of 20 gridpoints thickness are displayed (in red, green and blue respectively).

**Fig. 3** The advection of a bell shape out of computational domain moving parallel to PML $x$-direction: on the top left at 0 hour and top right at 24 hour forecast, on the bottom left at 36 hour and bottom right at 39 hour forecast.

**Fig. 4** Graph of the mean absolute divergence (in $\sec^{-1}$) for the case of advection of a bell shape out of computational domain moving parallel to PML multiplied by $10^8$. Case of no PML, large computational domain and a PML of 20 gridpoints thickness are displayed (in red, green and blue respectively).

**Fig. 5** The advection of a bell shape out of computational domain moving at angle of 45 degrees to PML $x$-direction: on the left at 24 hour and on the right at 36 hour forecast.

**Fig. 6** Graph of the mean absolute divergence (in $\sec^{-1}$) for the case of advection of a bell shape out of computational domain moving at an angle of 45° to PML multiplied by $10^8$. Case of no PML, large computational domain and a PML of 20 gridpoints thickness are displayed (in red, green and blue respectively).

**Fig. 7** The advection of the bell shape (2-D) out of the computational domain moving at an angle of 45° to PML: on the top left at 20 hour, on the top right at 60 hour forecast using 9 point filter. Simulation showing damping of unstable waves. On the bottom

at 60 hour forecast without using the 9 point filter. Simulation showing propagation of unstable waves in the PML.

**Fig. 8** Distribution of sigma within PML layer for the case of bell propagation at an angle of 45°

# Table Captions

**Table 1** Root-mean squared differences between a 48-hour forecast and the asymptotic solution given by the balanced state.

**Table 2** Root-mean squared difference between the 48 hour forecast and the analytical solution.

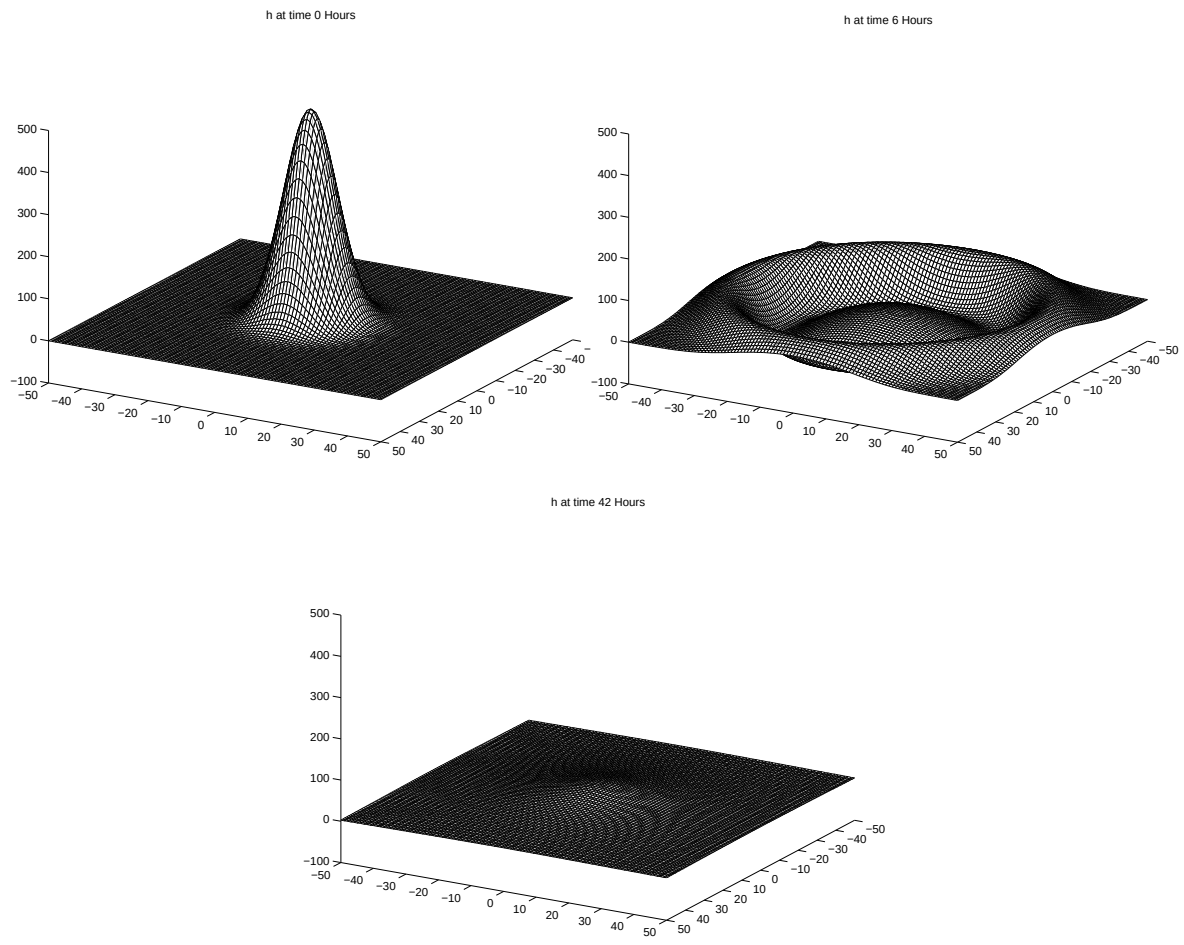


Figure 1: The adjustment of a bell shape using PML absorbing boundary condition: on the top left at 0 hour, on the top right at 24 hour forecast and on the bottom at 42 hour forecast.

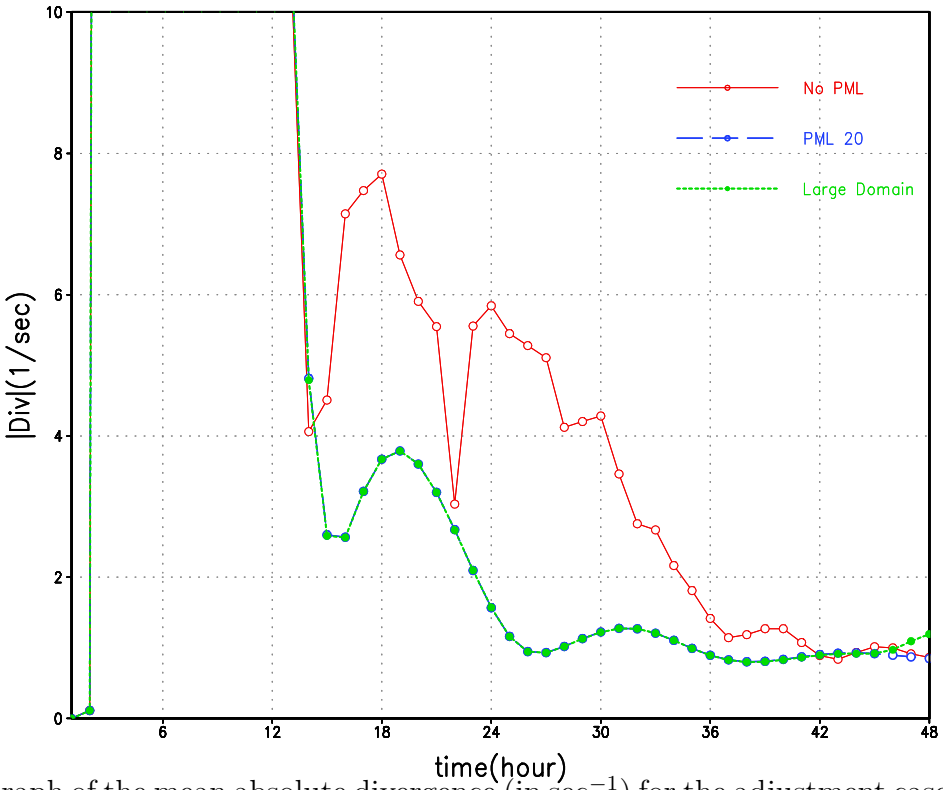


Figure 2: Graph of the mean absolute divergence (in $\sec^{-1}$) for the adjustment case multiplied by $10^8$. Case of no PML, large computational domain and a PML of 20 gridpoints thickness are displayed (in red, green and blue respectively).

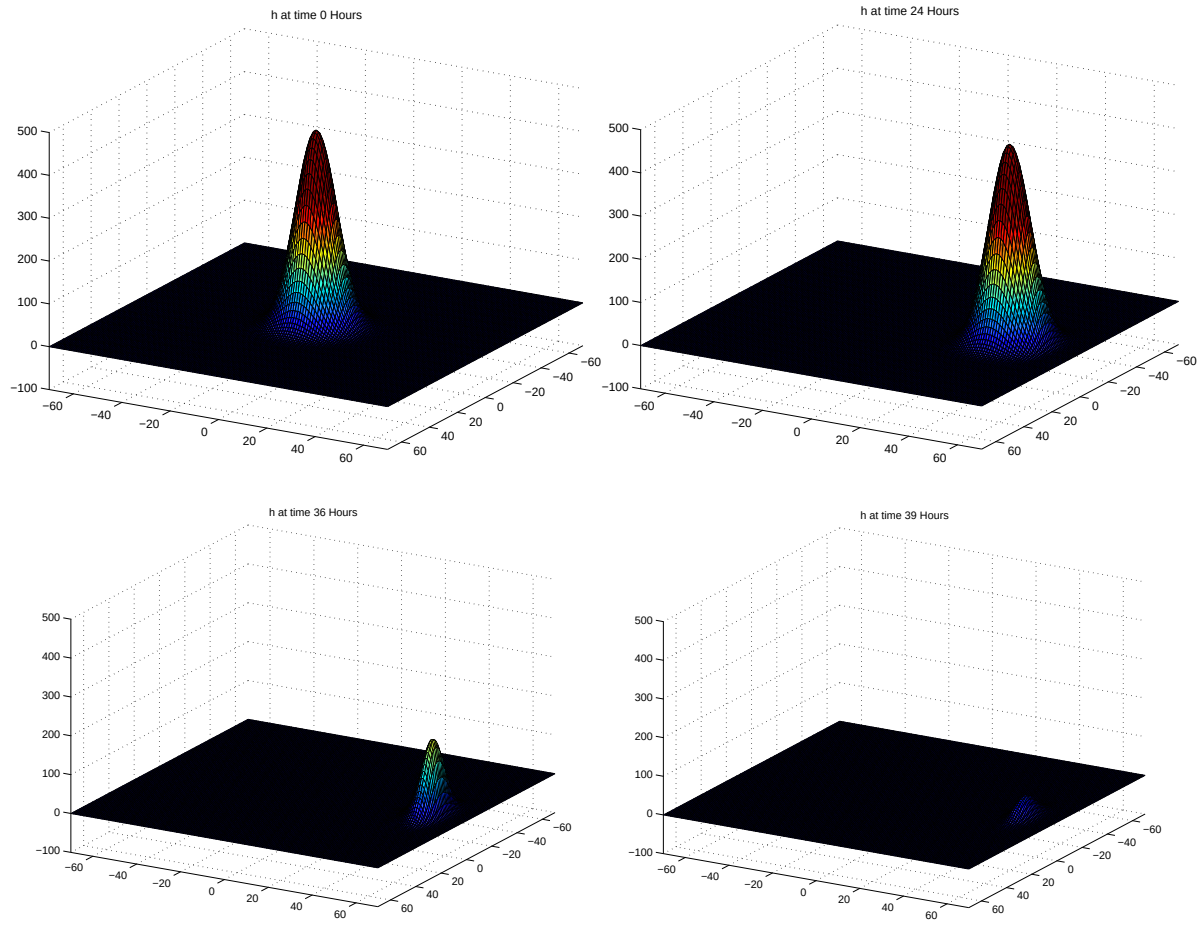


Figure 3: The advection of a bell shape out of computational domain moving parallel to PML $x$-direction: on the top left at 0 hour and top right at 24 hour forecast, on the bottom left at 36 hour and bottom right at 39 hour forecast.

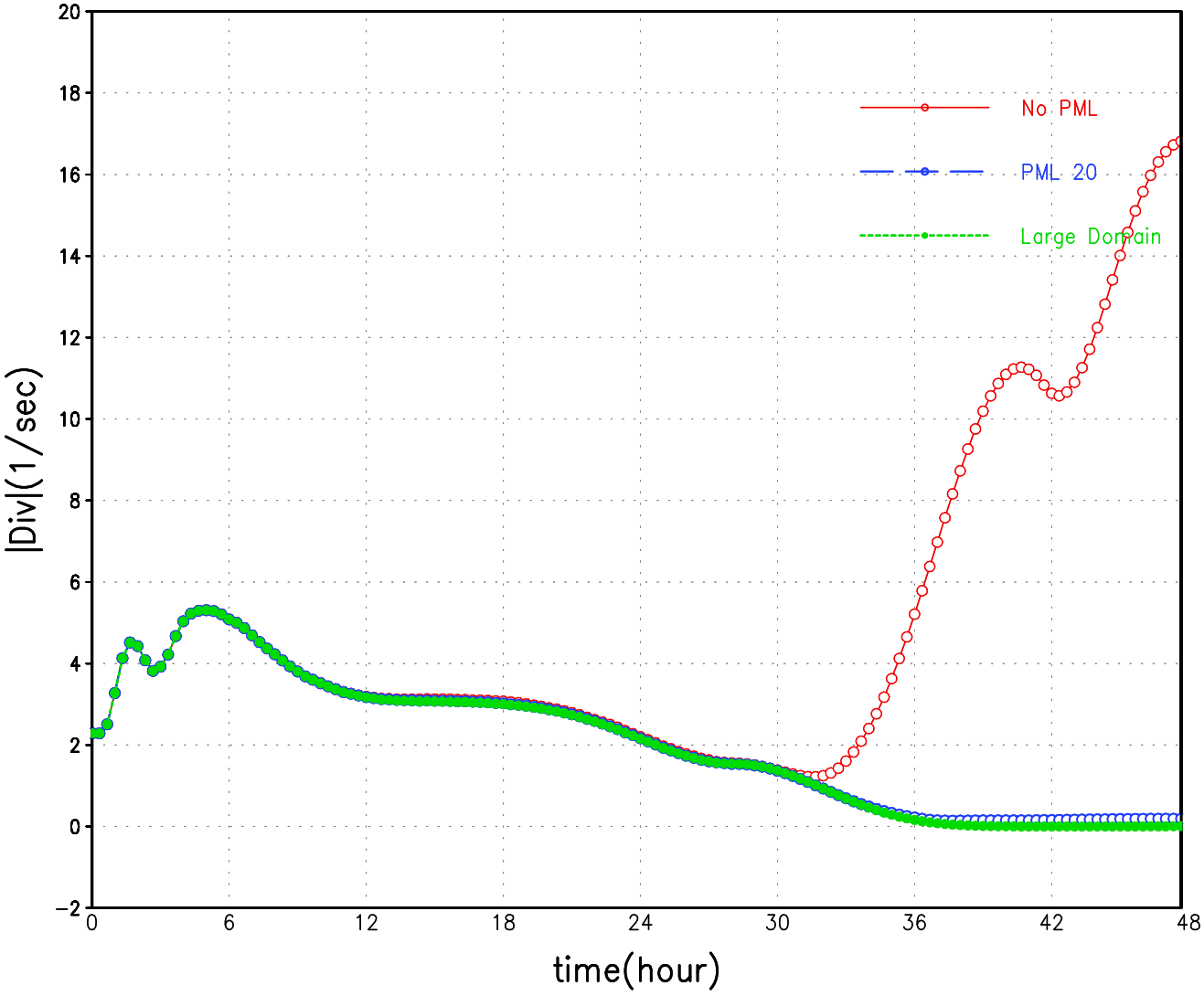


Figure 4: Graph of the mean absolute divergence (in $\sec^{-1}$) for the case of advection of a bell shape out of computational domain moving parallel to PML multiplied by $10^8$. Case of no PML, large computational domain and a PML of 20 gridpoints thickness are displayed (in red, green and blue respectively).

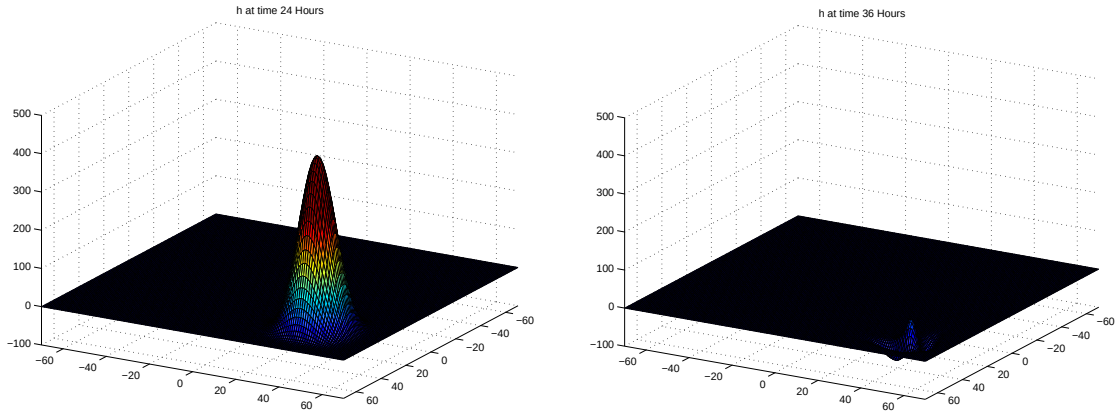


Figure 5: The advection of a bell shape out of computational domain moving at angle of 45 degrees to PML $x$-direction: on the left at 24 hour and on the right at 36 hour forecast.

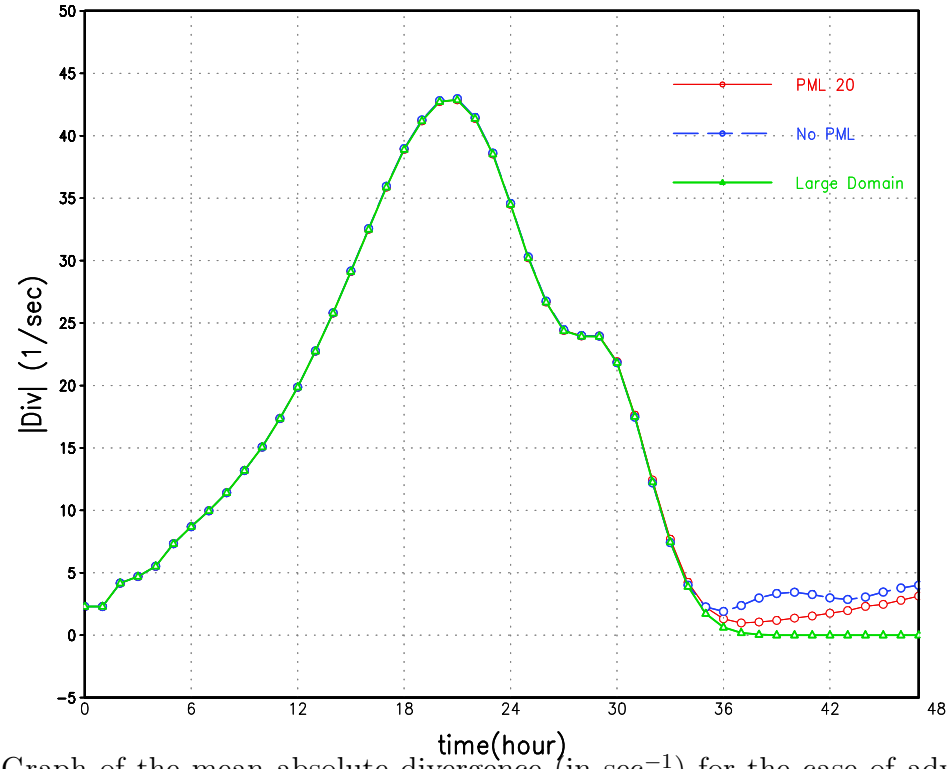


Figure 6: Graph of the mean absolute divergence (in $\sec^{-1}$) for the case of advection of a bell shape out of computational domain moving at an angle of 45° to PML multiplied by $10^8$. Case of no PML, large computational domain and a PML of 20 gridpoints thickness are displayed (in red, green and blue respectively).

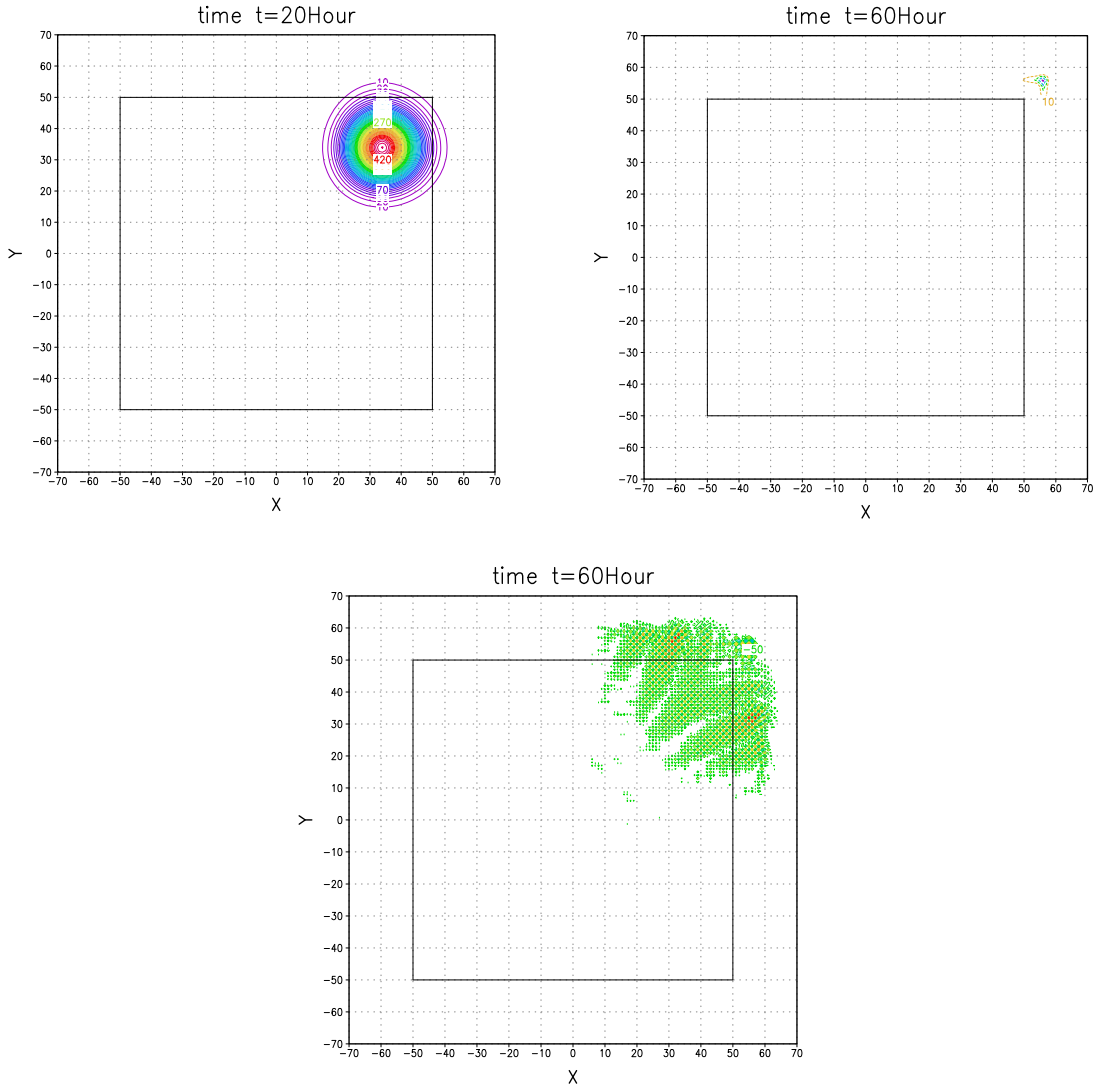


Figure 7: The advection of the bell shape (2-D) out of the computational domain moving at an angle of 45° to PML: on the top left at 20 hour, on the top right at 60 hour forecast using 9 point filter. Simulation showing damping of unstable waves. On the bottom at 60 hour forecast without using the 9 point filter. Simulation showing propagation of unstable waves in the PML.

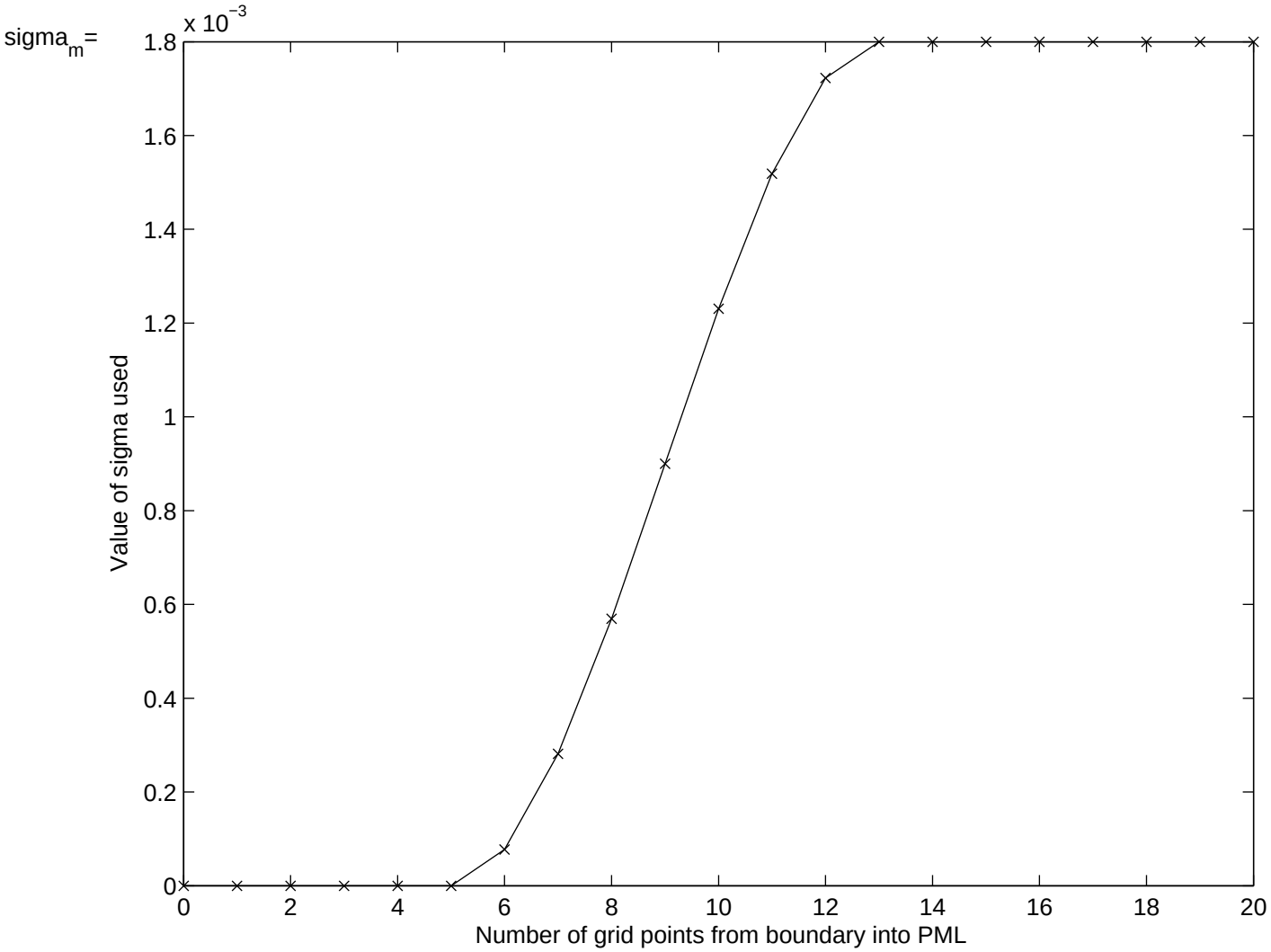


Figure 8: Distribution of sigma within PML layer for the case of bell propagation at an angle of 45°

Table 1: Root-mean squared differences between a 48-hour forecast and the asymptotic solution given by the balanced state.

| rms for h | rms for u | rms for v |
|---|---|---|
| 0.64 | 0.01 | 0.01 |

Table 2: Root-mean squared difference between the 48 hour forecast and the analytical solution.

| rms for h | rms for u | rms for v |
|---|---|---|
| 2.27 | 0.30 | 0.50 |